

RAPID COMMUNICATION

Mode-locked Tm-doped fiber laser with large modulation depth
ReS_{1.02}Se_{0.98} nanosheet saturable absorber

To cite this article: Yao Zhang *et al* 2019 *Jpn. J. Appl. Phys.* **58** 100907

View the [article online](#) for updates and enhancements.



Mode-locked Tm-doped fiber laser with large modulation depth ReS_{1.02}Se_{0.98} nanosheet saturable absorber

Yao Zhang^{1,3}, Junli Wang^{1,2*}, Mengyuan Ma¹, Chenxi Dou¹, Jiangfeng Zhu¹ , Guoqing Chang³, and Zhiyi Wei³

¹School of Physics and Optoelectronics Engineering, Xidian University, Xi'an 710071, People's Republic of China

²State Key Laboratory of Pulsed Power Laser Technology, Hefei 230037, People's Republic of China

³Beijing National Laboratory for Condensed Matter Physics, Institute of Physics, Chinese Academy of Sciences, Beijing 100190, People's Republic of China

*E-mail: dispersion@126.com

Received August 13, 2019; revised August 26, 2019; accepted August 30, 2019; published online September 19, 2019

In this paper, we demonstrate excellent ultrafast optical performance of ternary transition metal dichalcogenide ReS_{1.02}Se_{0.98} saturable absorber with high power tolerance and large modulation depth in thulium-doped fiber laser. Q-switching with tunable repetition frequency and pulse duration, and mode-locking with high pulse energy were generated in our experiment. The average output power/pulse energy/pulse duration of the mode-locked pulse train were 313 mW/13.6 nJ/1.43 ps, respectively. © 2019 The Japan Society of Applied Physics

Fiber lasers have many advantages, such as excellent thermal handling capability, better beam quality and higher optical conversion efficiency.¹⁾ In particular, ultrafast lasers with all-fiber structure have many unique applications.²⁾ In recent decades, all-fiber Q-switched and mode-locked lasers have been widely studied.^{3–5)} The ultrafast thulium-doped fiber (TDF) lasers locating at eye-safe wavelength range have attracted much attention, owing to their wide applications, such as biomedical treatment,^{6,7)} difference frequency generation,⁸⁾ free-space optical communications and national defense security, etc.

The methods for obtaining ultrashort pulse in fiber laser include nonlinear polarization evolution,⁹⁾ nonlinear optical loop mirror^{10,11)} and a series of saturable absorbers (SAs).¹²⁾ Because of the structural compactness for all-fiber integration, various kinds of SAs are been researched. They contain 1D carbon nanotubes and 2D materials ranging from graphenes,^{13–15)} topological insulators,^{16–18)} black phosphorus (BP),^{19–21)} to layered transition metal dichalcogenides (TMDs). Recently, various TMDs (MoS₂,²²⁾ WS₂,²³⁾ MoSe₂,^{24,25)} WSe₂,²⁶⁾ MoTe₂²⁷⁾ and ReS₂²⁸⁾ have been widely studied in the field of ultrafast optics. In 2018, Wang et al. first reported TDF mode-locked laser with MoTe₂-SA by the magnetron sputtering deposition method.²⁶⁾ Meanwhile, different regimes of solitons have also been reported with MoS₂ at 2 μm.²⁹⁾

The large modulation depth is helpful for obtaining shorter pulse duration and self-starting mode-locking pulses. In addition, SAs with high damage threshold are needed in many commercial applications. However, there have been few reports on high average power mode-locked fiber lasers harnessing large modulation depth SAs. Ternary ReS_{1.02}Se_{0.98} alloy, having environmental stability like common TMDs, can provide smaller energy band gap than ReS₂ with the single-atom dispersion layer,³⁰⁾ which indicates ReS_{1.02}Se_{0.98} is more suitable for applications at a longer wavelength. Besides, it has more freedom to regulate its energy band gap through not only adjusting the thickness of the atom dispersion layer, but by changing the proportion of two elements, for example, S and Se in the ReS_{2(1-x)}Se_{2x}.³¹⁾ Therefore, exploring the ultrafast optical properties of the ternary TMDs is more meaningful at eye-safe wavelength.

In this work, we employed ternary ReS_{1.02}Se_{0.98} film as an SA by mechanical exfoliation (ME) and obtained Q-switched and mode-locked operation in 2 μm regime. The appearance

and nonlinear saturable absorption characteristics of ReS_{1.02}Se_{0.98}-SA were investigated. Based on a high modulation depth of 39.9% and saturation intensity of 1.58 MW cm⁻² of ReS_{1.02}Se_{0.98}-SA, we demonstrated Q-switching with tunable pulse duration and repetition frequency from 8.54 μs/16.23 kHz to 5.38 μs/32.36 kHz and mode-locking at 1924 nm with pulse duration/pulse energy/average output power of 1.43 ps/13.6 nJ/313 mW, respectively. In our experiment, more mature and complete technologies of ME and material transfer enable our material to have better morphological uniformity compared with our previous work.^{32,33)} Besides, the photon energy in 2 μm is smaller than other shorter wavelength, which is conducive to the improvement of the tolerance of average power.

For obtaining high-quality 2D ReS_{1.02}Se_{0.98} film from bulk materials gathered together by van der Waals force, the direct, cost-effective and convenient method is ME. First, we used lengths of Scotch tape to peel the bulk materials repeatedly until we obtained a ReS_{1.02}Se_{0.98} film. Second, the ReS_{1.02}Se_{0.98} film was transferred from the lengths of tape to clean and tidy the quartz substrate. Finally, we employed a fiber connector (FC) to access the ReS_{1.02}Se_{0.98} film. With the help of van der Waals force, the film was attached to the end face of the FC, as shown in Fig. 1(a). And Fig. 1(b) is the microscope image of the FC. It can be seen that the fiber core was covered with a ReS_{1.02}Se_{0.98} film.

Then, we built a two-arm measurement device [Fig. 1(c)] to investigate the nonlinear optical properties of ReS_{1.02}Se_{0.98}-SA. The pump is a homemade pulse source. The output pulse string propagates through a variable optical attenuator and then is split by a 3 dB fiber coupler. Half of the power is measured by a power meter for reference, the rest of power is injected into the sample and then measured by a second power meter. The data of the transmission rate (blue points) of ReS_{1.02}Se_{0.98}-SA in the experiment is marked in Fig. 1(d). The red curve is the fitting result of experimental data by the following formula:

$$\alpha(I) = \alpha_{ns} + \frac{\alpha_s}{1 + I/I_{sat}}. \quad (1)$$

In formula (1), the modulation depth α_s , saturation intensity I_{sat} and nonsaturable loss α_{ns} are 39.9%, 1.58 MW cm⁻² and 48.6%, respectively. The large modulation depth is attributed to the morphological uniformity of the

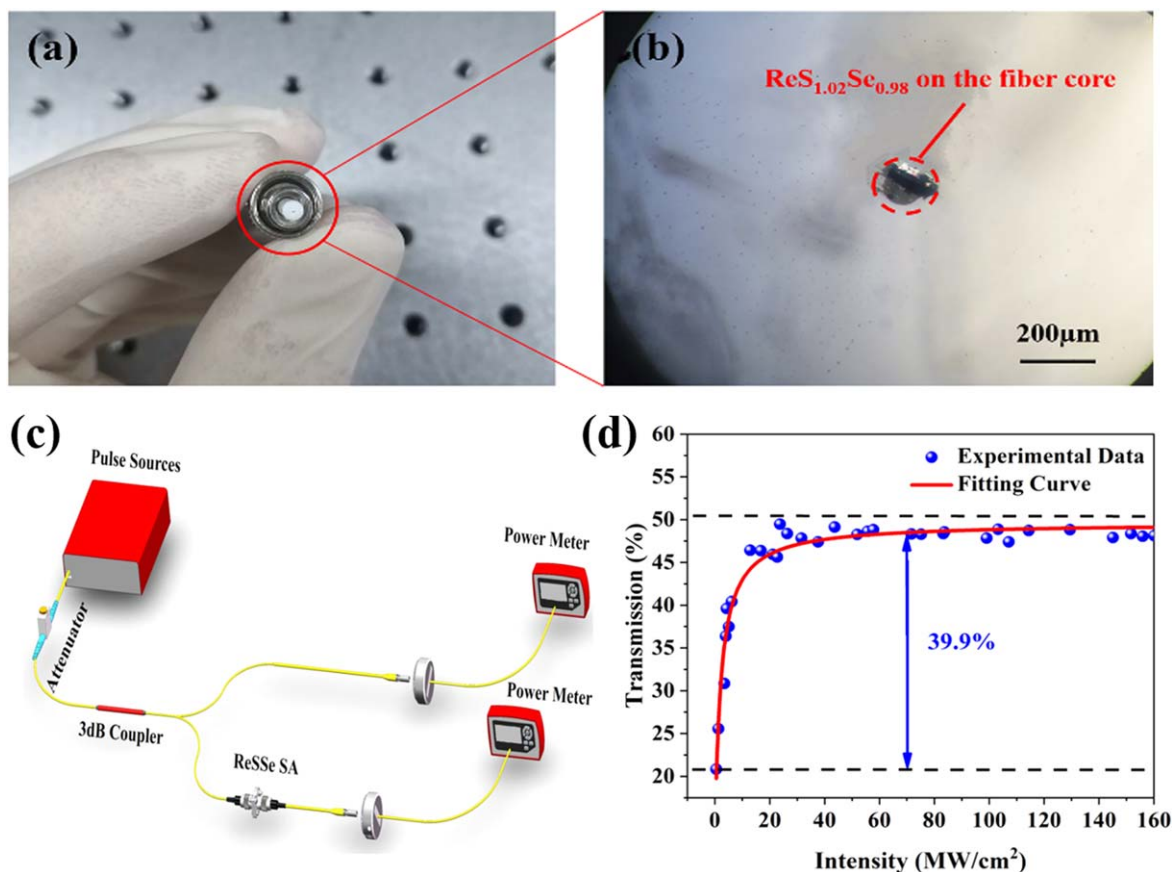


Fig. 1. (Color online) (a) Camera image of the FC. (b) Optical microscope image of the fiber core covered with a $\text{ReS}_{1.02}\text{Se}_{0.98}$ film. (c) Measurement setup. (d) Nonlinear absorption curve of $\text{ReS}_{1.02}\text{Se}_{0.98}$ -SA.

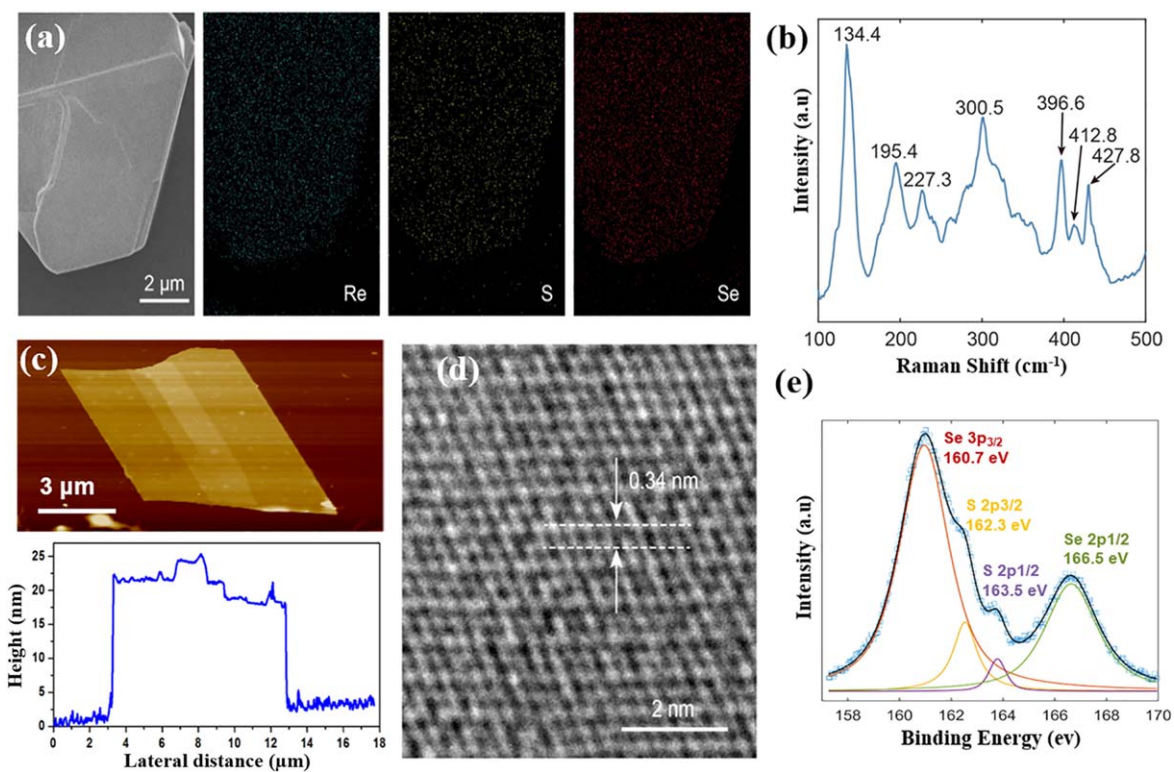


Fig. 2. (Color online) (a) SEM image and the mapping of Re, S and Se. (b) Raman spectrum of $\text{ReS}_{1.02}\text{Se}_{0.98}$ single crystal. (c) AFM topography and height diagram of a $\text{ReS}_{1.02}\text{Se}_{0.98}$ thin film on SiO_2/Si substrate. (d) HR-TEM image of a $\text{ReS}_{1.02}\text{Se}_{0.98}$ nanosheet. (e) XPS spectra.

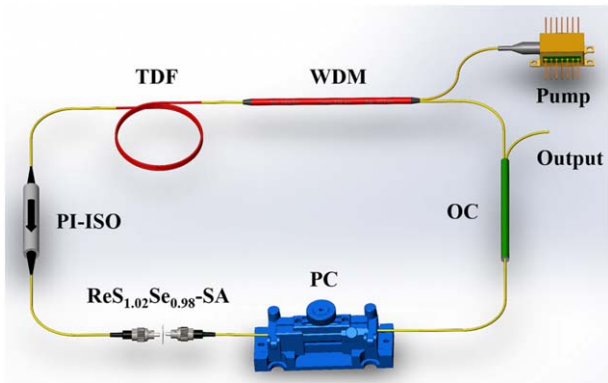


Fig. 3. (Color online) Schematic of the TDF laser.

ReS_{1.02}Se_{0.98} nanosheet, which can be observed by the following figures. Good uniformity of the materials not only gives a large surface-to-volume ratio, but yields a high saturation intensity and large modulation depth, as discussed in Ref. 34. High saturation intensity promotes high power operation and large modulation depth helps narrow the pulse.

The crystal structure and chemical composition of the fabricated ReS_{1.02}Se_{0.98} film are characterized in Fig. 2. The scanning electron microscopy (SEM) and energy dispersive spectroscopy images, respectively, are shown in Fig. 2(a). The elemental mapping of ReS_{1.02}Se_{0.98} shows a homogeneous distribution of Re, S and Se elements. The Raman spectrum [Fig. 2(b)] shows a series of peaks ranging from 100–500 cm⁻¹, which can be assigned to the Ag-like modes of ReS_{1.02}Se_{0.98}.³⁵ The atomic force microscopy (AFM)

image shows a representative 2D nanosheet with a height of about 20 nm in Fig. 2(c). The high-resolution transmission electron microscopy (HR-TEM) image [Fig. 2(d)] presents a set of lattice planes with a characteristic distance of 0.34 nm, corresponding to the distance of two Re atomic chains. The composition of the ReS_{1.02}Se_{0.98} nanosheet is confirmed by X-ray photoelectron spectroscopy (XPS). The peaks at 162.3, 163.5, 160.7 and 166.5 eV are attributed to the 2p^{3/2} and 2p^{1/2} orbitals of S²⁻ and 3p^{3/2} and 3p^{3/2} orbitals of Se²⁻, respectively, as shown in Fig. 2(e).

The principle of our system is shown in Fig. 3. A 1570 nm pump source with the maximum output power of 2 W is used to provide energy for the gain fiber by a 1570/2000 nm wavelength division multiplexing coupler. The 3 m long TDF (Nufern, SM-TSF-9/125; -77 ps² km⁻¹ @ 2.0 μm) with absorption coefficient ~14 dB m⁻¹ at 1570 nm is long enough to absorb the pump light adequately. A polarization-insensitive optical isolator is used to ensure unidirectional laser operation, and the ReS_{1.02}Se_{0.98} nanosheet is attached to the cavity by an optical fiber flange. A polarization controller (PC) was used to adjust the birefringence of the fiber. An output coupler (OC) with a splitting ratio of 50/50 was utilized to generate the output laser. The total length of this cavity is about 12 m, which consists of a 3 m long gain fiber and 9 m long fiber pigtail (SMF-28) with a group velocity delay of -71 ps² km⁻¹ at 2.0 μm.

The performance of the TDF laser was recorded by an InGaAs PIN photodetector, digital phosphor oscilloscope (Tektronix DPO 3054), optical spectrum analyzer (Miriad S3), autocorrelator (APE Pulsecheck), RF spectrum analyzer

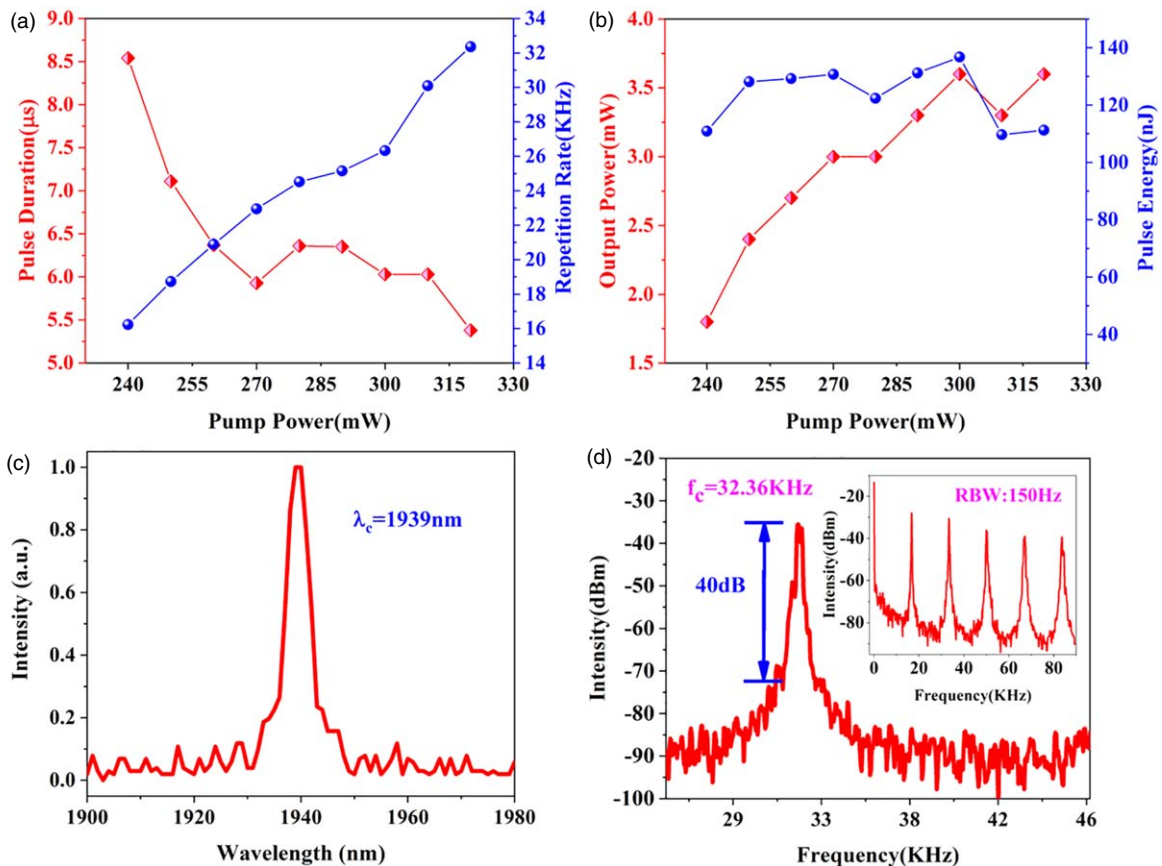


Fig. 4. (Color online) Q-switching performance of the TDF laser. (a) Repetition rate, pulse duration and (b) output power, single-pulse energy versus the pump power. (c) Spectrum at 270 mW. (d) RF spectrum at 320 mW.

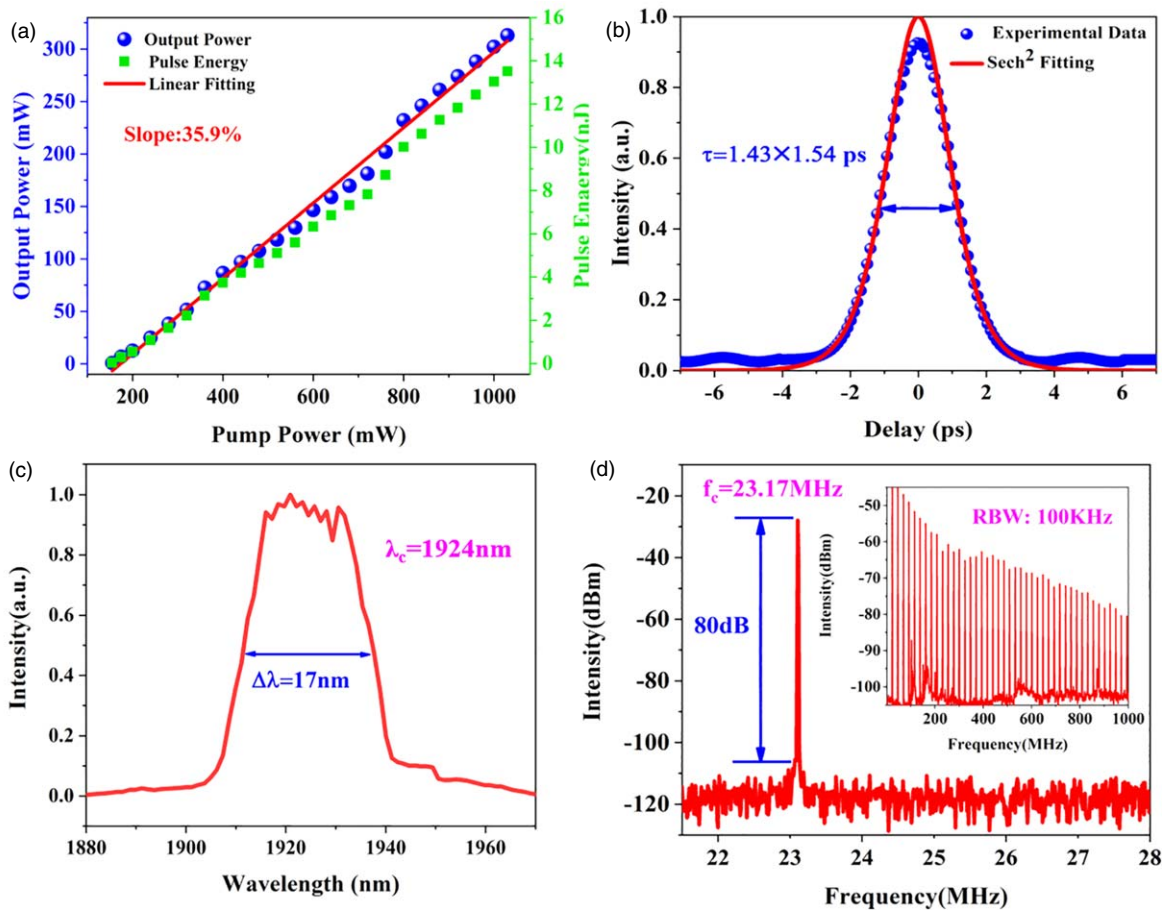


Fig. 5. (Color online) Output characterizations of the mode-locked TDF laser at 2 μm. (a) Characteristic curve of the output power and pulse energy. (b) Pulse duration. (c) Spectrum at 283 mW. (d) RF Spectrum.

(Rohde & Schwarz FSW) and power meter (LabMax-TOP, Coherent) through the output port of a 50/50 OC.

By changing the PC, self-generated Q-switching appears at the pump power of 240 mW. As shown in Fig. 4(a), when the pump power varies from 240–320 mW, the repetition rate increases from 16.23 to 32.36 kHz and the corresponding pulse width decreases from 8.54 to 5.38 μs. This presents the variation trend of output power and pulse energy. The output power increase from 1.8 to 3.6 mW with respect to pump power and the maximum pulse energy of 136.7 nJ are depicted in Fig. 4(b). Figure 4(c) shows the measured spectrum at the pump power of 270 mW. The center wavelength is 1939 nm. And Fig. 4(d) illustrates the RF spectrum at the pump power of 320 mW. The central frequency is 32.36 kHz with a signal-to-noise ratio (SNR) of 40 dB under the resolution bandwidth (RBW) of 50 Hz. The RF spectrum with 100 kHz span (RBW 150 Hz) is shown in the inset.

Then, we cut the passive fiber to change the dispersion of the total cavity and adjust the PC to optimize the birefringence and loss of fiber. The self-starting mode-locked operation is obtained at the pump power of 175 mW. Figure 5(a) shows the linear trend of the output power and pulse energy increase with pump power. The maximum average output power was measured to be 313 mW at pump power of 1030 mW, corresponding to pulse energy of 13.6 nJ. It is noted that the TDF laser is still stable in the pump range from 175–1030 mW at the fundamental

frequency. Once the pump power is beyond 1030 mW, multi-pulse operation is observed from the oscilloscope. Figure 5(b) is the autocorrelation trace of mode-locked pulse, and the pulse duration is calculated to be 1.43 ps under the fitting of sech². We infer that excessive negative chirp widens the output pulse. The optical spectrum at the pump power of 280 mW is depicted in Fig. 5(c). The center wavelength is located at 1924 nm with FWHM bandwidth around 17 nm. The resolution of our optical spectrum analyzer is greater than 1 nm, so the fine structure of the spectrum cannot be observed. Moreover, the 1570 nm pump light is not observed from the output spectrum. Figure 5(d) shows the RF spectrum with SNR of 80 dB under the RBW of 5 kHz. The frequency of the pulse string is 23.17 MHz, which is well matched with the value of the fundamental frequency. The inset is the RF spectrum with 1 GHz span under RBW of 100 kHz.

In our experiment, the main reason for the central wavelength of Q-switched operation being slightly larger than that of mode-locking is that the reabsorption effect caused by the long-wavelength laser in the emission spectrum of thulium ion is smaller, so as to balance the large loss in the cavity during Q-switched operation. In addition, we compare this work with other reports about mode-locked fiber lasers in 2 μm regime. As shown in Table I, we achieve the highest output power harnessing 2D materials, and the peak power of the mode-locked pulses is also higher than in most of the other works. This indicates that the ternary ReS_{1.02}Se_{0.98}-SA has the potential advantage in high-energy pulse fiber lasers.

Table I. Comparison of mode-locked TDF lasers at 2 μm harnessing 2D materials.

Year	SA	Output power (mW)	Pulse energy (nJ)	Pulse duration (ps)	Wavelength (nm)	Peak power (kw)	Modulation depth	References
2014	SPF-Bi ₂ Te ₃	1	0.055	0.795	1935	0.069	20.6%	36
2015	FF-BP	1.5	0.04	0.379	1910	0.107	4.1%	19
2017	FF-graphene	13	0.22	0.205	1945	1.073	13.9%	37
2017	MF-MTe ₂	39.3	2.13	1.25	1915	1.704	31.0%	35
2018	MF-MoTe ₂	212	13.8	1.3	1934	10.61	22.1%	26
2018	MF-WSe ₂	32.5	2.86	1.16	1863	2.465	1.83%	38
2018	FF-ReS _{1.02} Se _{0.98}	313	13.6	1.43	1924	9.49	39.9%	This work

FF: Fiber ferrule; MF: Microfiber; SPF: Side-polished fiber.

In summary, we report that Q-switching and mode-locking are obtained simultaneously at 2 μm based on ternary ReS_{1.02}Se_{0.98}-SA with high power tolerance and large modulation depth in TDF laser. At Q-switched operation, the repetition frequency and pulse duration are continuously tunable. For the mode-locked operation, the output power, pulse energy and center wavelength are 313 mW, 13.6 nJ and 1924 nm, respectively. The wavelength of this TDF laser is in the safe area of the human eyes. We believe the property of high power tolerance of ReS_{1.02}Se_{0.98} SA has great potential in biomedical applications.

Acknowledgments We thank Dr. Xin Chen for providing valuable assistance with this work. This work is partly supported by the National Key R&D Program of China (Grant No. 2018YFB1107200), the National Science Foundation of China (Grant Nos. 61675158, 21673058) and the Open Research Fund of the State Key Laboratory of Pulsed Laser Technology.

ORCID iDs Jiangfeng Zhu  <https://orcid.org/0000-0002-5515-8441>

- 1) W. Shi, Q. Fang, X. Zhu, R. A. Norwood, and N. Peyghambarian, *Appl. Opt.* **53**, 6554 (2014).
- 2) W. Fu, L. G. Wright, P. Sidorenko, S. Backus, and F. W. Wise, *Opt. Express* **26**, 9432 (2018).
- 3) M. Zhang, G. Hu, G. Hu, R. C. T. Howe, L. Chen, Z. Zheng, and T. Hasan, *Sci. Rep.* **5**, 11453 (2015).
- 4) Z. Wang, D. N. Wang, F. Yang, L. Li, C. Zhao, B. Xu, S. Jin, S. Cao, and Z. Fang, *J. Lightwave Technol.* **35**, 5280 (2017).
- 5) Z. Zhang, D. Popa, V. J. Wittwer, S. Milana, T. Hasan, Z. Jiang, A. C. Ferrari, and F. O. Ilday, *Appl. Phys. Lett.* **107**, 868 (2015).
- 6) D. Pal, A. Paul, N. Kr. Shekhar, S. D. Chowdhury, R. Sen, K. Chatterjee, and A. Pal, *IEEE J. Top. Quant.* **25**, 7100808 (2018).
- 7) M. D. Keller, J. A. Stafford, B. P. Schmidt, and J. D. Wells, *Proc. SPIE* **8207**, 820711 (2012).
- 8) G. Zhou, Q. Cao, F. X. Kärtner, and G. Chang, *Opt. Lett.* **43**, 2953 (2018).
- 9) D. G. Winters, M. S. Kirchner, S. J. Backus, and H. C. Kapteyn, *Opt. Express* **25**, 33216 (2017).
- 10) F. O. Ilday, F. W. Wise, and T. Sosnowski, *Opt. Lett.* **27**, 1531 (2002).
- 11) Y. Yu, H. Teng, H. Wang, L. Wang, J. Zhu, S. Fang, G. Chang, J. Wang, and Z. Wei, *Opt. Express* **26**, 10428 (2018).
- 12) K. Wu et al., *Opt. Commun.* **406**, 214 (2018).
- 13) G. Sobon, A. Duzynska, M. Świniarski, J. Judek, J. Sotor, and M. Zdrojek, *Sci. Rep.* **7**, 45491 (2017).
- 14) D. Popa, Z. Sun, F. Torrisi, T. Hasan, F. Wang, and A. C. Ferrari, *Appl. Phys. Lett.* **97**, 203106 (2010).
- 15) J. Sotor, J. Boguslawski, T. Martynkien, P. Mergo, A. Krajewska, A. Przewłoka, W. Strupiński, and G. Soboń, *Opt. Lett.* **42**, 1592 (2017).
- 16) H. Liu, X. W. Zheng, M. Liu, N. Zhao, A. P. Luo, Z. C. Luo, C. J. Zhao, and S. C. Wen, *Opt. Express* **22**, 6868 (2014).
- 17) Y. H. Lin, C. Y. Yang, S. F. Lin, W. H. Tseng, Q. Bao, C. I. Wu, and G. R. Lin, *Laser Phys. Lett.* **11**, 055107 (2014).
- 18) J. Sotor, G. Sobon, W. Macherzynski, and K. M. Abramski, *Laser Phys. Lett.* **11**, 055102 (2014).
- 19) J. Sotor, G. Sobon, M. Kowalczyk, W. Macherzynski, P. Paletko, and K. M. Abramski, *Opt. Lett.* **40**, 3885 (2015).
- 20) Y. Chen et al., *Opt. Express* **23**, 12823 (2015).
- 21) Z. C. Luo, M. Liu, Z. N. Guo, X. F. Jiang, A. P. Luo, C. J. Zhao, X. F. Yu, W. C. Xu, and H. Zhang, *Opt. Express* **23**, 20030 (2015).
- 22) R. I. Woodward, E. J. R. Kelleher, R. C. T. Howe, G. Hu, F. Torrisi, T. Hasan, and J. R. Taylor, *Opt. Express* **22**, 31113 (2014).
- 23) B. Guo, Q. L. Yu, Y. Yao, and P. F. Wang, *Opt. Mater. Express* **6**, 2475 (2016).
- 24) B. H. Chen, X. Y. Zhang, K. Wu, H. Wang, J. Wang, and J. P. Chen, *Opt. Express* **23**, 26723 (2015).
- 25) H. Xia, H. Li, C. Lan, C. Li, X. Zhang, S. Zhang, and Y. Liu, *Opt. Express* **22**, 17341 (2014).
- 26) J. Yin et al., *Opt. Express* **25**, 30020 (2017).
- 27) J. Wang, Z. Jiang, H. Chen, J. Li, J. Yin, J. Wang, T. He, P. Yan, and S. Ruan, *Photonics Res.* **6**, 535 (2018).
- 28) D. Mao, X. Cui, X. Gan, M. Li, W. Zhang, H. Lu, and J. Zhao, *IEEE J. Sel. Top. Quantum Electron.* **24**, 1100406 (2018).
- 29) P. Wang, K. Zhao, L. Gui, X. Xiao, and C. Yang, *IEEE Photonic. Tech. L.* **30**, 1210 (2018).
- 30) W. Wen et al., *Small* **13**, 1603788 (2017).
- 31) W. Wen, J. Lin, K. Suenaga, Y. Guo, Y. Zhu, H.-P. Hsu, and L. Xie, *Nanoscale* **9**, 18275 (2017).
- 32) C. Dou, W. Wen, J. Wang, M. Ma, L. Xie, C. H. Ho, and Z. Wei, *Photonics Res.* **7** (2019).
- 33) M. Ma, W. Wen, Y. Zhang, C. Dou, J. Wang, L. Xie, C. H. Ho, and Z. Wei, *J. Mater. Chem. C* **7**, 6900 (2019).
- 34) R. Wei, H. Zhang, X. Tian, T. Qiao, Z. Hu, Z. Chen, X. He, Y. Yu, and J. Qiu, *Nanoscale* **8**, 7704 (2016).
- 35) J. Wang, Z. Jiang, H. Chen, J. Li, J. Yin, J. Wang, T. He, P. Yan, and S. Ruan, *Opt. Lett.* **42**, 5010 (2017).
- 36) M. Jung, J. Lee, J. Koo, J. Park, Y.-W. Song, K. Lee, S. Lee, and J. H. Lee, *Opt. Express* **22**, 7865 (2014).
- 37) J. Sotor, J. Boguslawski, T. Martynkien, P. Mergo, A. Krajewska, A. Przewłoka, W. Strupiński, and G. Soboń, *Opt. Lett.* **42**, 1592 (2017).
- 38) J. Wang et al., *IEEE J. Sel. Top. Quantum Electron.* **24**, 1100706 (2017).